The Journal of Chemical Physics ARTICLE pubs.aip.org/aip/jcp

Shaping membrane vesicles by adsorption of hinge-like nanoparticles

Cite as: J. Chem. Phys. 160, 194901 (2024); doi: 10.1063/5.0204225
Submitted: 20 February 2024 • Accepted: 29 April 2024 •
Published Online: 15 May 2024

View Online Export Citation CrossMark

Bing Li[1] and Steven M. Abel[2,a)]

AFFILIATIONS

[1] State Key Laboratory of Polymer Physics and Chemistry, Changchun Institute of Applied Chemistry, Chinese Academy of Sciences, 130022 Changchun, China
[2] Department of Chemical and Biomolecular Engineering, University of Tennessee, Knoxville, Tennessee 37996, USA

[a)] **Author to whom correspondence should be addressed:** abel@utk.edu

ABSTRACT

The adsorption of particles onto fluid membranes can lead to membrane-mediated interactions between particles that promote their self-assembly and lead to changes in membrane morphology. However, in contrast with rigid particles, relatively little is known about deformable particles, which introduce additional complexities due to the mutual deformability of the particles and the membrane. Here, we use Monte Carlo simulations and umbrella sampling to investigate the equilibrium properties of hinge-like particles adsorbed on membrane vesicles by means of anisotropic, attractive interactions. We vary the hinge stiffness, adhesive area fraction, patterning of adhesive regions, and number of adsorbed particles. Depending on their properties, isolated particles can conform to the vesicle, induce invaginations of the membrane, or exhibit multistable behavior in which they sample distinct classes of configurations due to the interplay of particle and membrane deformations. With two adsorbed particles, the properties of the particles can be used to promote aggregation, bias the particles to different parts of the vesicle, or stabilize the coexistence of both cases. With multiple adsorbed particles, the number and type control their organization and collective impact on the vesicle, which can adopt shapes ranging from roughly spherical to dumbbell-like and multi-lobed. Our results highlight how modifying the mechanical properties and patterned adhesion of deformable particles, which is possible with DNA nanotechnology, influences their self-assembly and the resulting shapes of both the particles and vesicles.

Published under an exclusive license by AIP Publishing. https://doi.org/10.1063/5.0204225

15 May 2024 15:20:43

I. INTRODUCTION

Cell membranes enclose cells and organelles, exhibit diverse morphologies, and are frequently remodeled to transform their shape and topology. Membrane remodeling is a fundamentally important process in living cells, contributing, for example, to endocytosis, viral budding, and cell division. Various membrane-deforming proteins, which can sense and generate membrane curvature, play a crucial role in the formation and stabilization of membrane shapes.[1–11]

DNA nanotechnology, due to its versatility and programmability, has emerged as a useful means to modify membrane properties and remodel membrane morphologies.[12–17] DNA origami nanostructures, when decorated with lipid moieties, can anchor to lipid membranes and induce curvature.[18–20] Lipid membranes, in turn, can drive the assembly of DNA nanostructures to minimize the bending energy of the membrane. For example, curved DNA origami nanostructures designed to mimic BAR (Bin-Amphiphysin-Rvs)-family proteins, when anchored to vesicles by cholesterol, can collectively cause membrane deformations that lead to structures such as membrane tubules. The nature and degree of deformation depend on the curvature of the particles and the positions of the cholesterol anchors.[21] Rod-like DNA origami nanoparticles anchored on lipid membranes can also experience membrane-mediated attractive interactions between particles, which results in their self-organization.[22]

Much theoretical and simulation work has focused on membrane deformations induced by the assembly of rigid particles adsorbed on membranes.[23–28] Linear aggregates of spherical particles have been observed in simulations due to the attractive interactions between particles when they come close to one another.[24,29] For particles adsorbed on the inside[25] or outside[26] of a vesicle, the particles can assemble into linear aggregates enclosed by membrane tubules protruding out of or into the vesicle. Recent simulations of

Published under an exclusive license by AIP Publishing

spherical Janus nanoparticles adsorbed on vesicles further show that the interactions between particles depend on the curvature of the vesicles from the perspective of the particles. When the membrane initially curves away from the particles, they experience attractive interactions, but when the membrane curves toward the particles, they experience repulsive interactions.[28] Other recent studies have considered the self-assembly of Janus nanoparticles on planar membranes and vesicles.[30–32] On planar membranes, the adsorbed particles form an ordered hexagonal superlattice at intermediate area number density and intermediate to high adhesion strength.[31] On vesicles, highly ordered assemblies of particles can be tuned by varying the number of adsorbed particles, the relative size between particles and vesicles, and the adhesion strength.[32]

For axisymmetric particles, membrane-mediated interactions between particles depend on the adsorption strength. When the attraction of particles to the membrane is weak, the particles repel each other.[33] When the attraction is strong, the interaction between particles is attractive and can lead to large deformations of the membrane and the alignment of elongated particles. Both rod-like and curved particles tend to form tip-to-tip aggregates to lower the membrane bending energy.[34–37] The nature of the aggregation also depends on the membrane tension: Tip-to-tip aggregation is favored at low tension, while side-by-side aggregation is favored at higher tension.[38] The assembly behavior of curved particles can deform vesicles into different morphologies, such as faceted, disk, tube, and bud.[39–42] Bonazzi *et al.* further studied membrane morphologies induced by curved nanoparticles binding along either their concave or convex sides and revealed that convex-side binding can stabilize three-way junctions of membrane tubules.[43]

A recent development in DNA nanotechnology is the design of DNA origami nanostructures with tunable mechanical properties, as exemplified by hinge-like nanoparticles.[44,45] Structures with programmed deformability provide an exciting building block for mechanically functional DNA origami devices and materials,[46] and studying their interactions with deformable surfaces such as lipid membranes is particularly interesting because the particles and surface can mutually deform one another. Deformable, hinge-like structures can also be found in proteins such as melittin and the antimicrobial peptide LL-37, which have been implicated in curvature sensing. Coarse-grained simulations revealed that melittin and LL-37, each of which contains two α-helices joined in a hinge-like configuration, have the ability to detect direction-dependent curvature.[47] Noguchi recently studied the curvature sensing of proteins with asymmetric shapes and structural deformations using a model consisting of two crescent, rod-like segments connected by a kink.[48] Hinge-like peptides further motivate the investigation of the adsorption of deformable particles on membranes. However, there is a limited understanding of how deformable particles interact with membranes and how their mechanical properties influence their membrane-mediated interactions and self-assembly.[49]

In previous work, we investigated two hinge-like particles adsorbed onto a planar membrane by means of a non-directional, short-range attractive potential between the particle and the membrane. We characterized how the membrane-mediated interactions depend on the adsorption strength and hinge stiffness.[50] However, the effects of directional attractive potentials, closed membrane vesicles, and multiple particles are still unknown. We are interested in the effects of directional interactions because, experimentally, nanoparticles with both nonadhesive and strongly adhesive areas have been realized by spatially patterning cholesterol anchors.[21,51] To address this gap, we consider a model system of hinge-like particles comprised of beads with an adhesive cap with an area fraction of x. To simulate membrane anchors being on different facets of DNA origami nanostructures, we group the hinge particles into two types: *concave* particles where the adhesive caps are on the side with an acute angle, and *convex* particles where the adhesive caps are on the other side. We first use unbiased Monte Carlo simulations to characterize the effects of hinge type, hinge stiffness, and adhesive area fraction for isolated particles and pairs of particles adsorbed on a membrane. We further use umbrella sampling to investigate the potential of mean force between two particles and reveal the dependence of their interaction on these factors. We finally study the organization of multiple particles and the resulting membrane shapes induced by the particles.

II. MODEL AND SIMULATION DETAILS

We consider a fluid membrane vesicle, which is modeled as a triangulated, self-avoiding, and closed surface consisting of $M = 828$ spherical hard beads of diameter $l_{mem} = \sigma$ connected by bonds with lengths ranging from σ to 1.67σ. The membrane bending energy is given by[52–54]

$$E_{mem} = \sqrt{3}\kappa \sum_{\langle i,j \rangle} (1 - \mathbf{n}_i \cdot \mathbf{n}_j), \tag{1}$$

where κ is the bending rigidity of the membrane, $\mathbf{n}_i$ denotes the normal vector to triangle i, and the sum is over all triangles i and j sharing an edge. In our work, we fix $\kappa = 10k_BT$. Membrane fluidity is introduced by bond-flip moves in simulations, so the connectivity is not fixed.[50,54–56] The energy cost associated with area changes is included via the term $E_\gamma = \gamma A$, where γ is the surface tension and A is the total surface area. In our work, γ is set to $1k_BT/\sigma^2$. For σ corresponding to a length scale of ~30 nm, the surface tension is of the order 10^{-3}–10^{-2} pN/nm.[24,50,57] The bounds on the lengths of individual bonds restrict the minimum and maximum surface area possible.

The hinge particle is represented by two connected rods comprised of Janus-like particles. Each arm of the hinge consists of three hard-sphere beads of diameter $l_r = 2\sigma$ connected by fixed-length bonds of length 2.02σ. The center bead is shared by the two arms. The surface of each bead is divided into a strongly adhesive cap (Fig. 1, red portion) with an area fraction of x and a nonadhesive cap (Fig. 1, blue portion) with an area fraction of $1 - x$. The adhesive area fraction of each bead is $x = (1 - \cos\phi)/2$, where the characteristic angle ϕ is the angle between the vector from the bead center to the center point of the adhesive cap and the vector from the bead center to points at the edge of the cap. Here, we consider $\phi = \pi/4$ and $\pi/2$, which correspond to $x = 0.146$ and 0.5, respectively. The center of the attractive cap is placed on each bead to form either convex particles, with the caps on the outer surface of the hinge, or concave particles, with the caps on the inner surface (Fig. 1). We use the terms concave and convex by analogy with other work on curved nanoparticles.[43] In previous work, we tested the relative size of the particle beads to the membrane beads[50] and found that $l_r = 2l_{mem}$

15 May 2024 15:20:43

Published under an exclusive license by AIP Publishing

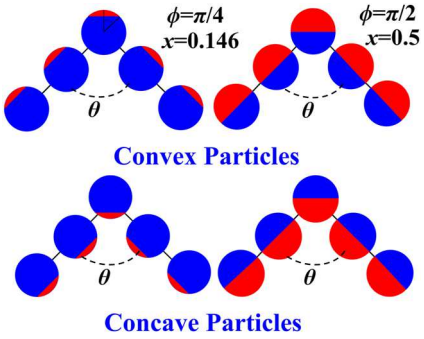

FIG. 1. Schematic of the four hinge-like particles studied. The hard-sphere beads comprising the particle are divided into a strongly adhesive cap (red) with an area fraction of x and a nonadhesive region (blue) with an area fraction of $1 - x$. For convex particles, the adhesive caps are on the outer part of the hinge. For concave particles, the adhesive caps are on the inner part of the hinge.

was sufficiently large so that the discretization of the membrane did not impact the configurations adopted by the membrane or particles. This choice of relative particle size is also consistent with the work of others.[38]

The attractive interaction between a hinge bead and a vesicle bead is modeled via a generic power-law potential if the line connecting the center of the membrane bead and the center of the hinge bead passes through the adhesive cap; it is zero otherwise. The attractive power-law potential between hinge bead i and membrane bead j is[25,50]

$$E_{ad,ij} = -D_0\left(\frac{l_{\min}}{r_{ij}}\right)^6, \tag{2}$$

where $l_{\min} = (l_{mem} + l_r)/2$, r_{ij} is the distance between the beads, and a cutoff is imposed at $r_{cut} = 1.5l_{\min}$. The total adhesion energy E_{ad} is the sum over all pairs of i and j. Here, $D_0 = 15k_BT$, which corresponds to the strong adsorption regime. In experiments, DNA origami nanoparticles with strongly adhesive and nonadhesive surface areas have been realized by spatially patterning lipid moieties that anchor to lipid membranes.

The angle between the two arms of a hinge particle is denoted by θ. The bending energy of the hinge is given by[50]

$$E_h = k_\theta(\theta - \theta_0)^2, \tag{3}$$

where k_θ is the hinge stiffness and θ_0 is the preferred hinge angle. In this work, θ_0 is set to $\pi/2$, and the value of k_θ is varied to simulate hinges with different degrees of flexibility.

We perform Metropolis Monte Carlo computer simulations to sample configurations of the system at thermal equilibrium. For membranes, there are two types of trial Monte Carlo (MC) moves: single-particle displacement moves and bond-flip moves. Details are presented in previous work.[50,56,58] For hinge particles, we use two types of pivot moves:[50,59,60] One is a global pivot move in which an entire hinge particle is rotated by a random angle around the axis through a randomly selected bead with random orientation. The other is a local pivot movement where one rod of a particle is randomly selected and rotated by a random angle around the axis through the common bead of two rods and normal to the plane the hinge lies in. All trial moves are accepted or rejected according to the standard Metropolis criterion, and the simulations satisfy detailed balance. Each Monte Carlo step (MCS) consists of M attempted displacement moves, M attempted bond-flip moves, 100 attempted global pivot moves, and 100 attempted local pivot moves.

We first equilibrate the system for 1×10^6 MCS without attractive interactions between particles and the membrane. We then include attractive membrane–particle interactions and use a simulated annealing method to obtain reliable sampling. The value of D_0 is increased from $D_0 = 8k_BT$ to $15k_BT$ with an increment of $\delta D = 0.5k_BT$. At each increment, we relax the system for 1×10^6 MCS. Upon reaching the target value of D_0, we relax the system for an additional 5×10^6 MCS before collecting data. We perform 1×10^7 MCS in each collection run and store the configuration every 5×10^3 MCS. Ten independent simulation trajectories are generated for each set of conditions. For stiff, convex particles with a small adhesive area fraction, we discovered that one arm would adhere to the vesicle but the other would only rarely adsorb (4 out of 50 independent trajectories in a trial to assess the sampling). However, once two arms were in contact, they never detached from the membrane, and the total average energy with both arms in contact was favorable compared to configurations with only one in contact. These simulations suggest that an energy barrier hinders the adsorption of the second arm and, thus, the sampling of equilibrium configurations with two arms adsorbed. This is in contrast with other hinge types, where both arms readily adsorb. For stiff hinges, to overcome the barrier and focus on the fully adsorbed configurations, we initialize the simulations with configurations obtained from simulations of weak hinges in which both arms are adsorbed to the vesicle. We then follow the same annealing and sampling procedures described above.

We also employ umbrella sampling simulations to calculate the potential of mean force (PMF) as a function of the distance between two hinges adsorbed on a vesicle.[50,60–64] Here, a harmonic bias potential, $\omega_b = k(r - r_0)^2$, is used, with r denoting the distance between the centers of mass of the two hinges. The spring constant is $k = 200k_BT/\sigma^2$. We divide the reaction coordinate $r \in [0, r_{\max}]$ into 60 windows with different r_0, where $r_{\max} = 20\sigma$ for particles with large adhesive area fraction and $r_{\max} = 26\sigma$ for particles with a small adhesive area fraction. We use the umbrella integration method[61] to obtain the unbiased probability distribution and calculate the change in free energy along the reaction coordinate (r). The minimum value of the free energy is set to zero. The membrane bending energy, adsorption energy, and total energy are also calculated by averaging configurations falling into the neighborhood of each window center, $r \in [r_0 - \delta, r_0 + \delta]$, where $2\delta = 0.2\sigma$ is the bin width.

III. RESULTS AND DISCUSSION

A. Single particle: Impact of hinge type, hinge stiffness, and adhesive area fraction

We first study a single hinge particle adsorbed on a vesicle and characterize its equilibrium configurations in terms of the hinge angle θ. For an isolated particle without a vesicle, θ is approximately normally distributed with a mean value of $\theta_0 = \pi/2$.[50] When the hinge adsorbs on a vesicle, the incompatibility of the natural angle of the hinge and the curvature of the vesicle leads to changes in

15 May 2024 15:20:43

Published under an exclusive license by AIP Publishing

the distribution of θ because the hinge and vesicle mutually deform one another. The deformations depend on the interplay between the energy of deforming the hinge, which depends on its stiffness, and the energy of deforming the membrane. Due to the large size of the vesicle compared with the particle, highly flexible hinges are expected to increase their hinge angle to conform to the vesicle surface. Stiffer hinges, in contrast, are expected to exhibit less pronounced deformations while inducing larger deformations of the vesicle.[50]

Figures 2(a) and 2(b) show the probability density of the hinge angle (θ) for different values of hinge stiffness (k_θ) and adhesive area fraction (x). For convex particles [Fig. 2(a)], when the adhesive area fraction is small $(x = 0.146)$ and the hinge is weak $(k_\theta = 15k_BT)$, the distribution is narrow with a peak at $\theta \approx 0.92\pi$. As shown in the accompanying snapshot, this corresponds to a straightening of the hinge and a relatively minor alteration of the vesicle shape. For the stiffer hinge $(k_\theta = 45k_BT)$, the peak occurs at $\theta \approx 0.75\pi$ because of the larger cost of deforming the particle. The vesicle is moderately deformed inward to conform to the shape of the hinge.

When the adhesive area fraction is large $(x = 0.5)$, the vesicle and hinge adopt more deformed configurations to promote favorable contact. The distribution of θ for the weak hinge changes substantially, with the emergence of two peaks: The more prominent peak is located at $\theta \approx 0.75\pi$, where the hinge adopts a bent configuration and is partially wrapped by the membrane to form an inward bud. The second peak at $\theta \approx 0.90\pi$ corresponds to a straighter hinge accommodated by a cleft in the vesicle surface. This bimodal distribution reflects the interplay between the energy to deform the particle and the energy to deform the membrane. For more bent hinge configurations, the bending energy of the membrane is relatively large but is compensated by a relatively low hinge deformation energy. For straighter hinge configurations, the energy of the particle is relatively large but is compensated by a relatively low membrane bending energy. Thus, the balance between deforming the hinge and membrane leads to two prominent classes of configurations at

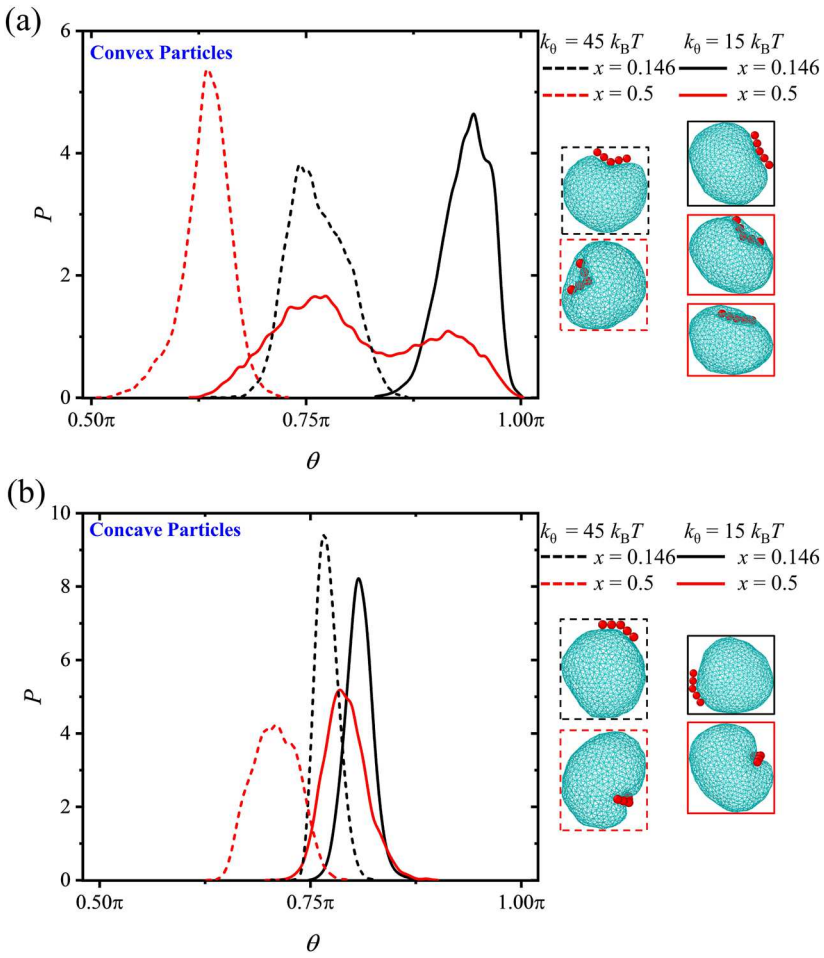

FIG. 2. Probability density (P) of the hinge angle (θ) for different values of the hinge stiffness (k_θ) and area fraction (x) for a single convex (a) and concave (b) particle adsorbed on a vesicle. Characteristic snapshots associated with peaks in the distributions are shown for each case. The box framing each snapshot identifies the associated hinge stiffness (solid or dashed) and adhesive area fraction (black or red). The preferred angle of the hinge is $\theta_0 = \pi/2$.

15 May 2024 15:20:43

Published under an exclusive license by AIP Publishing

equilibrium, as reflected by the bimodal distribution. Furthermore, the distribution of the hinge angle can be tuned by varying the stiffness of the hinge. For the stiffer hinge, the minor peak disappears, and the location of the major peak shifts toward smaller values ($\theta \approx 0.63\pi$). Here, the vesicle is further deformed to form an inward bud. For a weaker hinge with $k_\theta = 5k_BT$, the major peak associated with the bent particle disappears, and the location of the minor peak shifts toward higher values (Fig. S1).

For concave particles [Fig. 2(b)], it is easier for the hinge to conform to the vesicle, leading to less deformation of both the hinge and vesicle. When the adhesive area fraction is small, the shape of the vesicle is not significantly changed by the adsorption of the particle, and both weak and strong hinges exhibit some degree of straightening to coincide with the curvature of the vesicle. For the larger adhesive area fraction, the hinge induces larger changes in the shape of the vesicle, which adopts a cashew-like shape with the hinge at the "waist" of the vesicle for both values of the hinge stiffness. Similar configurations have been reported for a semiflexible polymer adsorbed on a vesicle in previous work.[56] The peak of the distribution of θ occurs at smaller angles for stiffer hinges.

B. Two particles: Spatial distribution and membrane shape

The results in Fig. 2 demonstrate how particle type, hinge stiffness, and adhesive area fraction impact the configurations of hinges and vesicles when a single particle is adsorbed. Because membrane deformations can lead to effective interactions between hinges, we consider two particles adsorbed on a vesicle and characterize the distribution of the distance r between their centers of mass.

We first consider the case of convex particles, which induce inward budding of vesicles at the larger adhesive area fraction. Figures 3(a) and 3(b) show the probability density of r. For $x = 0.5$, the peak of the distribution occurs near $r = 10\sigma$ for both values of the hinge stiffness. As shown in the snapshots, this corresponds to the particles being at the opposite sides of a strongly deformed vesicle. In contrast, for $x = 0.146$, the distribution reveals two stable configurations: The peak at large r corresponds to the particles located on opposite sides of a pear-shaped vesicle. The peak at small r corresponds to particles in side-by-side contact on a cashew-shaped vesicle. For weaker hinge stiffness, the particles are more likely to be

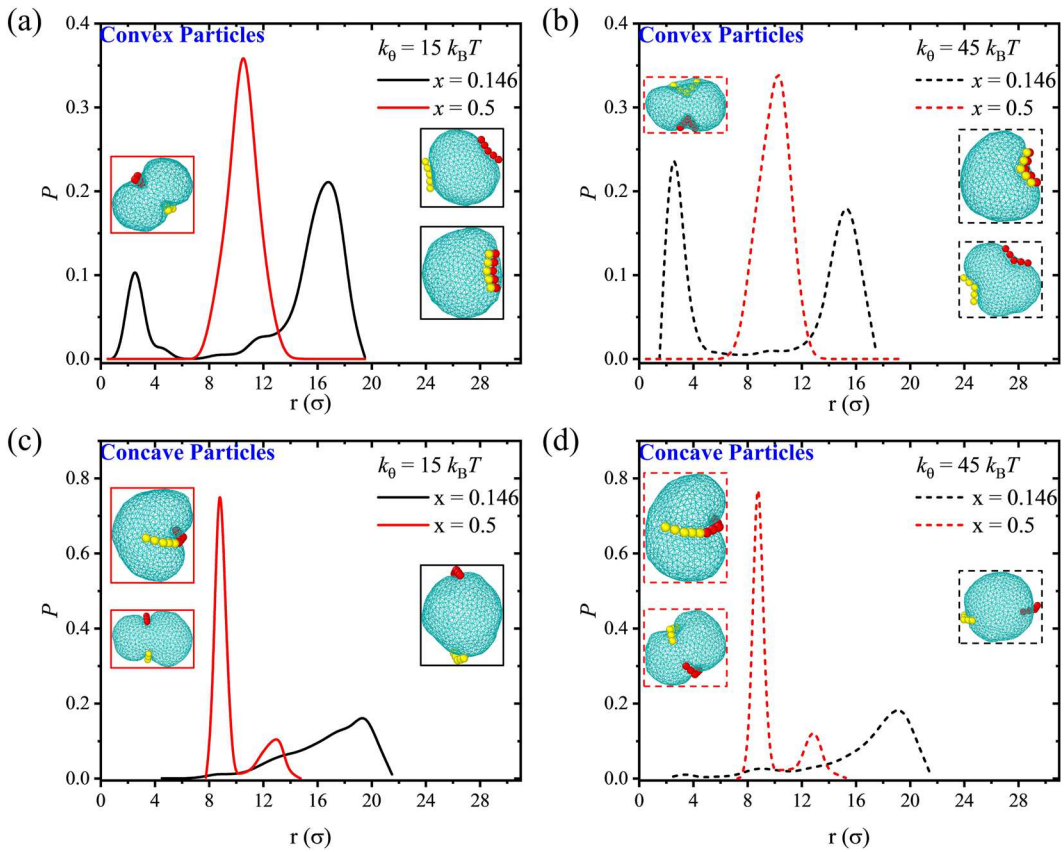

FIG. 3. Probability density (P) of the distance (r) between the centers of mass of two particles adsorbed on a vesicle for different values of the hinge stiffness (k_θ) and adhesive area fraction (x). (a) and (b) Results for convex particles. (c) and (d) Results for concave particles. Characteristic snapshots associated with peaks in the distributions are shown for each case. The box framing each snapshot identifies the associated hinge stiffness (solid or dashed) and adhesive area fraction (black or red).

15 May 2024 15:20:43

Published under an exclusive license by AIP Publishing

in the configuration in which they are separated. For stronger hinge stiffness, the side-by-side configuration is more prominent. Thus, increasing the hinge stiffness can promote side-by-side aggregation of convex particles with a small adhesive area fraction.

For concave particles, which induce less pronounced deformation of vesicles, the distribution of r exhibits qualitatively different behavior from that of convex particles [Figs. 3(c) and 3(d)]. For $x = 0.146$, the distribution is relatively broad with a peak near $r = 19\sigma$, which is approximately the diameter of the vesicle. The corresponding snapshots show two particles on opposite sides of a minimally deformed vesicle. For $x = 0.5$, the major peak of the distribution is located near $r = 8.5\sigma$, where the two particles form an end-to-end aggregate and induce a cashew-like vesicle shape. The minor peak near $r = 13\sigma$ corresponds to a configuration where the two particles are located at opposite sides of the waist of a "cinched" vesicle. The hinge stiffness has less influence on the behavior of concave particles than on convex particles.

C. Two particles: Effective interactions

To quantify the effective, membrane-mediated interactions between two particles adsorbed on a vesicle, we use the umbrella integration method[61] to characterize the potential of mean force (PMF), $\Delta F = F(r) - F_{\min}$, as a function of the distance (r) between the centers of mass of the two particles. We report the PMF relative to its minimum value in the range of interest, $F_{\min}$.

1. Convex particles

Figure 4 shows the PMFs obtained for convex particles. For $x = 0.146$, the weaker hinges give rise to two minima located near $r = 3\sigma$ and 17σ [Fig. 4(a)], with the local minimum near $r = 17\sigma$ having a lower effective free energy. The stiffer hinge also has two local minima [Fig. 4(b)], but in contrast, the minimum near $r = 3\sigma$ corresponds to the lower effective free energy. Thus, the larger hinge stiffness favors the aggregation of convex particles with small adhesive patches. For $x = 0.5$, the PMF exhibits a single minimum, which occurs near $r = 10\sigma$ for both values of the hinge stiffness. As shown in Fig. 3, this corresponds to the hinges being on opposite sides of a highly deformed vesicle.

For further insight into the two convex particles, we analyze contributions to the total energy as a function of r (Fig. 5). When $x = 0.146$ and $k_\theta = 15k_BT$ [Fig. 5(a)], the total energy is relatively flat for $6\sigma < r < 18\sigma$ when compared to the variation in the PMF. This indicates that the minimum in the PMF near $r = 17\sigma$ is entropically favorable. As r decreases from 6σ, the total energy first increases but then exhibits a local minimum near $r = 3\sigma$. When $x = 0.146$ and $k_\theta = 45k_BT$ [Fig. 5(b)], the total energy has a minimum near $r = 3\sigma$ and increases with increasing r. The favorable entropic contribution at large r is offset by the energetic cost, leading to the minimum in the PMF at small r being the most favorable state.

When $x = 0.5$, weak and strong hinges have a minimum in the total energy near $r = 9\sigma$ and $r = 10\sigma$, respectively [Figs. 5(c) and 5(d)]. These minima are consistent with the minima observed in the PMFs. To explore why the particles do not adopt a closer configuration such as the side-by-side configurations observed for $x = 0.146$, we analyze the energetic contributions and snapshots of the system. At smaller values of r, the membrane energy increases with decreasing r [Figs. 5(c) and 5(d)] because the curvature of the membranes between the hinges increases (Fig. 6). The large bending energy outweighs the favorable change in adhesion energy. Near $r = 5\sigma$, the membrane bending energy and adhesion energy exhibit a sharp change for $k_\theta = 15k_BT$ [Fig. 5(c)] but not for $k_\theta = 45k_BT$ [Fig. 5(d)]. This corresponds to the straightening of at least one hinge (Fig. 6). This leads to a decrease in the bending energy but comes at the expense of less adhesive contact between the hinge and the membrane. Physically, the particles do not come into side-by-side contact because doing so would lead to a substantial loss of adhesive contact; the highly curved membrane shapes observed in Fig. 6 are energetically unfavorable but allow the particles to maintain a large contact area.

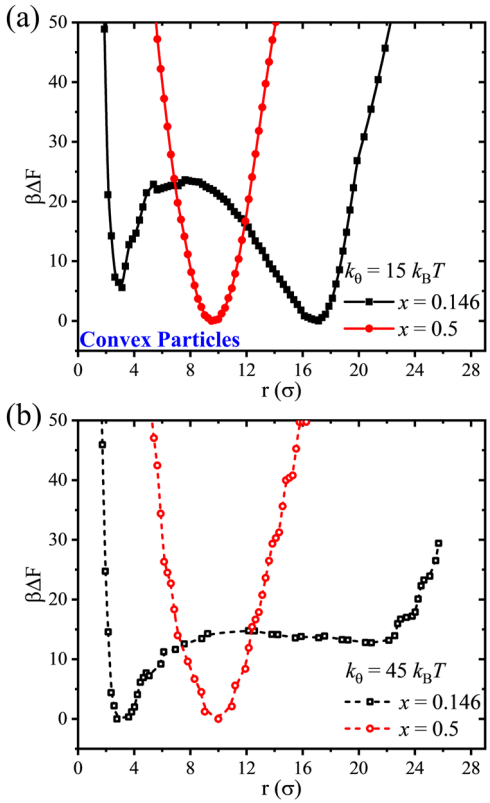

FIG. 4. Potential of mean force (ΔF) as a function of the distance (r) between the centers of mass of two convex hinges for different values of the adhesive area fraction and hinge stiffness: (a) $k_\theta = 15k_BT$ and (b) $k_\theta = 45k_BT$.

2. Concave particles

Figure 7 shows the PMFs obtained for concave particles. For $x = 0.146$ and $k_\theta = 15k_BT$, the PMF has a single minimum near $r = 19\sigma$. In contrast, the stiffer hinge has three local minima. The global minimum is near $r = 19\sigma$, with additional local minima near $r = 9\sigma$ and 3σ. These two minima correspond to end-to-end and side-by-side configurations, respectively, although the side-by-side configuration is extremely unlikely and hence physically inconsequential. For $x = 0.5$ and $k_\theta = 15k_BT$, the PMF has two minima located near $r = 9\sigma$ and 14σ, with the end-to-end configuration $(r \approx 9\sigma)$ corresponding to the lowest free energy. The stiffer hinge

15 May 2024 15:20:43

Published under an exclusive license by AIP Publishing

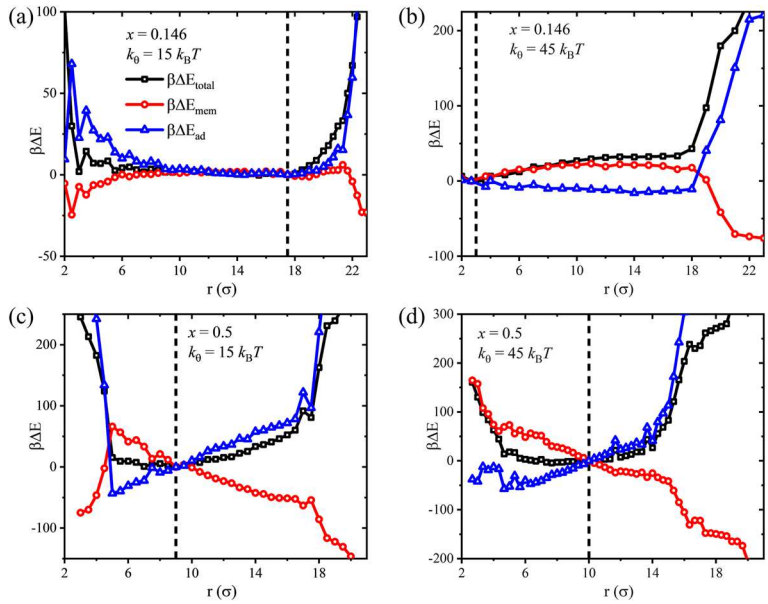

FIG. 5. Change in the total energy (ΔE_{total}), membrane bending energy (ΔE_{mem}), and adhesion energy (ΔE_{ad}) as functions of the distance (r) between the centers of mass of two convex hinges. ΔE denotes the change in energy relative to the energy at the distance where the total energy is smallest (dashed line). (a) $x = 0.146$, $k_\theta = 15k_BT$; (b) $x = 0.146$, $k_\theta = 45k_BT$; (c) $x = 0.5$, $k_\theta = 15k_BT$; and (d) $x = 0.5$, $k_\theta = 45k_BT$.

has two primary minima near $r = 9\sigma$ and 13σ. However, the end-to-end configuration ($r \approx 9\sigma$) is more favored when compared with the weak hinge.

Figures 8(a) and 8(b) show the energy as a function of r for $x = 0.146$. The total energy is approximately constant in the region of $6\sigma \le r \le 22\sigma$ for both $k_\theta = 15k_BT$ and $45k_BT$, indicating that the minima in the PMFs near $r = 19\sigma$ and $r = 9\sigma$ are entropically favorable. For $x = 0.5$, the total energy has a minimum at $r = 9\sigma$ [Figs. 8(c) and 8(d)], in agreement with the global minimum of the PMF. The total energy first increases as r increases from $r = 9\sigma$, but then flattens in the range $12\sigma < r < 14\sigma$ before increasing again.

Note that the PMFs for convex and concave particles (Figs. 4 and 7) are generally consistent with the distributions of r obtained from unbiased simulations (Fig. 3); peaks in Fig. 3 correspond to minima in the PMFs. However, the PMFs provide quantitative information about the relative free energy of various states that would require far longer simulation time in unbiased simulations. The one notable inconsistency between the results is for convex particles with $x = 0.146$ and $k_\theta = 45k_BT$. In this case, there is a peak in the distribution of r near $r = 15.5\sigma$, but the associated local minimum in the PMF is near $r = 22.5\sigma$. This can be attributed to the fact that the biasing potential used in umbrella sampling caused one of the arms

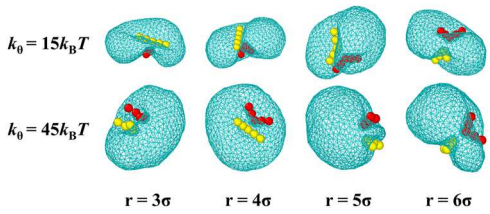

FIG. 6. Snapshots of configurations of two convex particles at various separation distances (r) with $x = 0.5$.

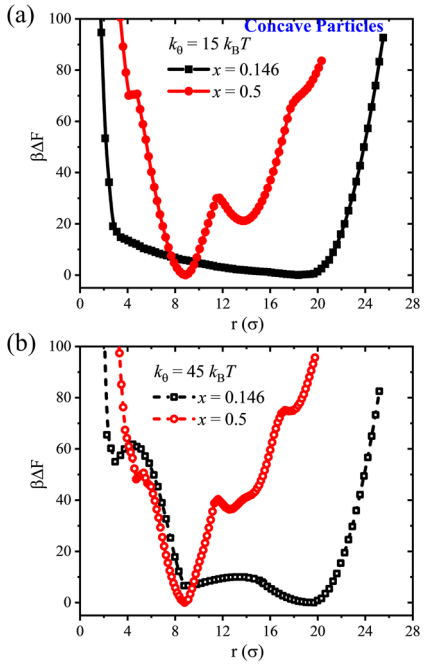

FIG. 7. Potential of mean force (ΔF) as a function of the distance (r) between the centers of mass of two concave hinges for different values of the adhesive area fraction and hinge stiffness: (a) $k_\theta = 15k_BT$ and (b) $k_\theta = 45k_BT$.

15 May 2024 15:20:43

Published under an exclusive license by AIP Publishing

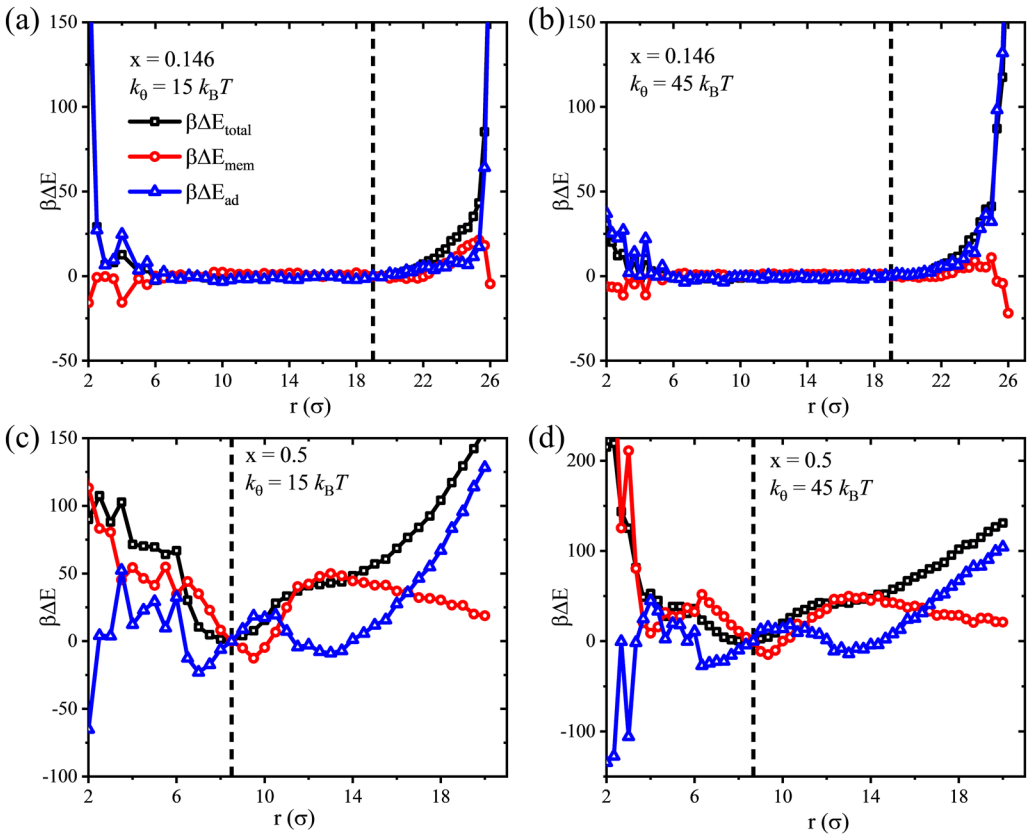

FIG. 8. Change in the total energy (ΔE_{total}), membrane bending energy (ΔE_{mem}), and adhesion energy (ΔE_{ad}) as functions of the distance (r) between the centers of mass of two concave hinges. ΔE denotes the change in energy relative to the energy at the distance where the total energy is smallest (dashed line). (a) $x = 0.146$, $k_\theta = 15k_BT$; (b) $x = 0.146$, $k_\theta = 45k_BT$; (c) $x = 0.5$, $k_\theta = 15k_BT$; and (d) $x = 0.5$, $k_\theta = 45k_BT$.

of the hinge to dissociate from the vesicle, whereas in unbiased simulations, the hinges maintained full contact for the duration of the simulations. This is consistent with our trial simulations indicating an energy barrier separating configurations with one and both arms in contact with the vesicle (see Sec. II). The broad minimum in the PMF likely results from the two stable classes of configurations, but the barrier to one arm's dissociation is not clearly evident along the reaction coordinate used for the PMFs.

D. Multiple particles: Collective behavior

Thus far, we have shown how hinge stiffness (k_θ), adhesive area fraction (x), and particle type (convex vs concave) impact the behavior of single particles and pairs of particles adsorbed on a vesicle. In this section, we characterize the membrane-mediated organization of multiple particles adsorbed on a vesicle and their impact on the shape of the vesicle. We consider cases with $N = 4$ and 10 particles.

Figure 9 shows representative equilibrium snapshots of multiple hinges adsorbed on a vesicle. For convex particles with $x = 0.146$ and $k_\theta = 15k_BT$ [Fig. 9(a)], the hinges have little influence on the vesicle for $N = 4$. The particles straighten to gain favorable contact with the surface, but the shape of the vesicle does not markedly change. Increasing the number of particles leads to the self-assembly of the particles and substantial deformation of the vesicle. With $N = 10$, two stable configurations are observed: In one, the vesicle is dumbbell-shaped with particles surrounding the narrow "waist" in a side-by-side configuration. In the other, three distinct groups of particles in side-by-side contact sculpt the vesicle into the shape of a three-way junction. Increasing the hinge stiffness leads to the particles having a more pronounced impact on the shape of the vesicle. For $N = 4$, the particles aggregate and lead to a cashew-like vesicle shape. For $N = 10$, the particles aggregate in a side-to-side configuration and deform the vesicle into a dumbbell-like shape. The neck connecting the two lobes is narrower than with $k_\theta = 15k_BT$ due to the smaller hinge angle.

For convex particles with $x = 0.5$ [Fig. 9(b)], both weak and strong hinges cause invaginations of the membrane around the particles. This is energetically unfavorable from the perspective of membrane bending, but it increases the contact area between the particles and the membrane. Similar behavior has been observed

15 May 2024 15:20:43

Published under an exclusive license by AIP Publishing

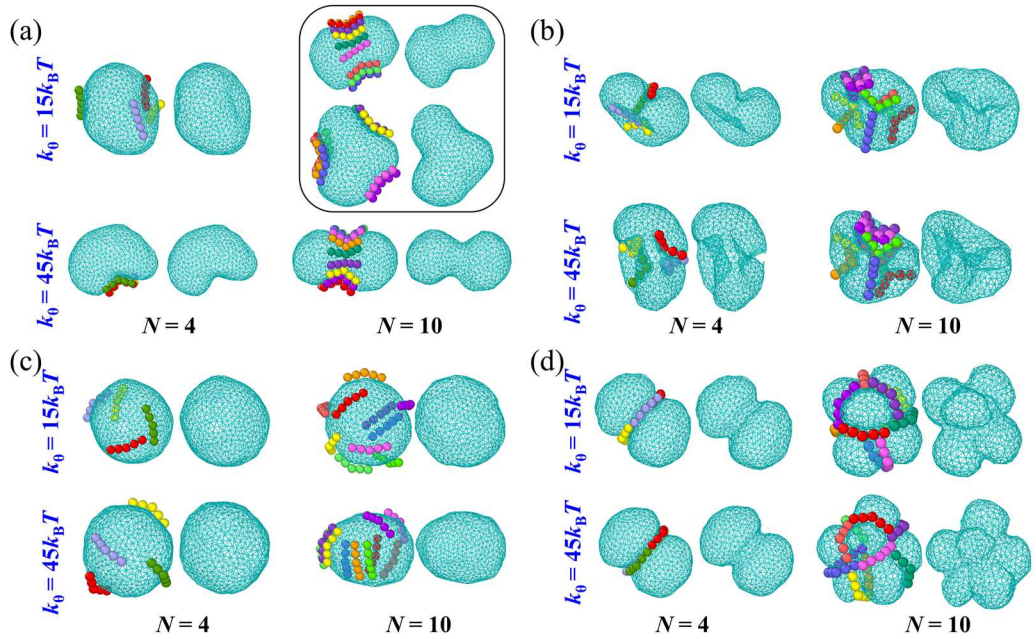

FIG. 9. Snapshots of multiple particles adsorbed on a vesicle. Four cases are shown in each panel and correspond to different values of the hinge stiffness (k_θ) and number of hinges (N). For each case, the left image shows the particles on the vesicle, and the right image shows the same snapshot without particles to more clearly reveal deformations of the vesicle. (a) Convex particles with $x = 0.146$. The boxed configurations for $k_\theta = 15k_BT$ and $N = 10$ correspond to two distinct states observed. (b) Convex particles with $x = 0.5$. (c) Concave particles with $x = 0.146$. (d) Concave particles with $x = 0.5$.

for semiflexible polymers, which can form inward buds when adsorbed to vesicles.[56] When the number of hinges increases from $N = 4$ to 10, more particles aggregate together to form larger invaginations.

For concave particles with $x = 0.146$ [Fig. 9(c)], the hinges do not markedly impact the shape of the vesicles. For $k_\theta = 15k_BT$, the shape of the vesicle is largely unchanged for both $N = 4$ and $N = 10$, and the hinges are distributed around the surface. For

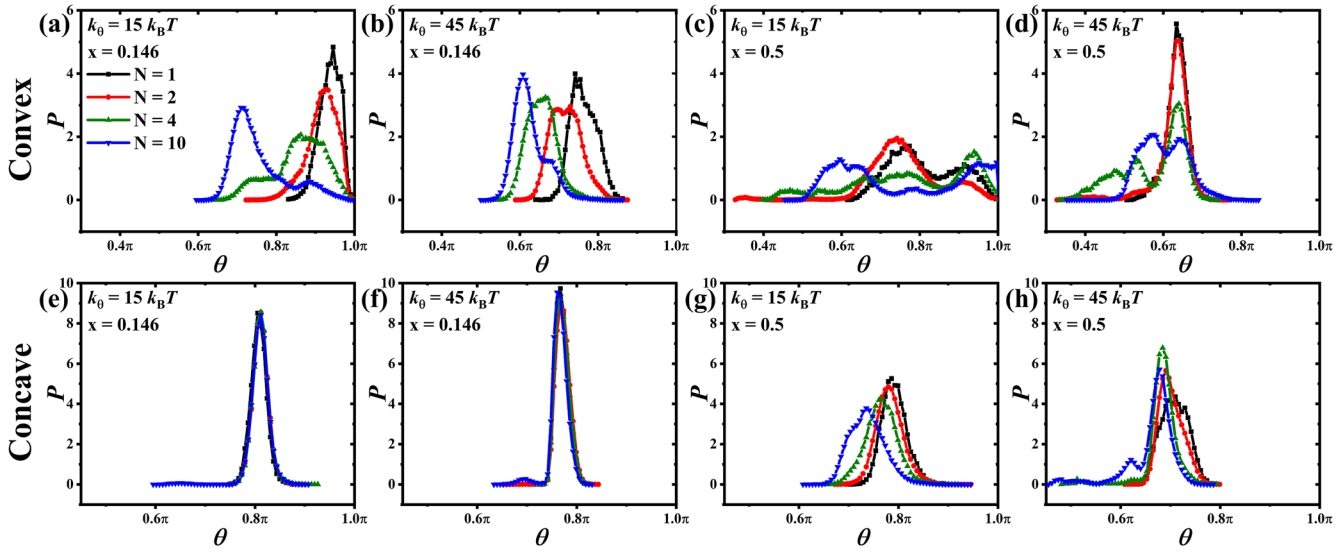

FIG. 10. Probability density (P) of the hinge angle (θ) for different values of the hinge stiffness (k_θ) and adhesive area fraction (x) for multiple convex (a)–(d) and concave (e)–(h) particles adsorbed on a vesicle.

15 May 2024 15:20:43

Published under an exclusive license by AIP Publishing

$k_\theta = 45k_BT$ and $N = 10$, the particles promote an oblate membrane shape, with the hinges preferentially located near the equator. For $x = 0.5$ [Fig. 9(d)], the particles tend to induce furrow-like deformations of the membrane and assemble in end-to-end configurations. With $N = 4$ particles, the vesicle adopts a dumbbell-like shape with particles circling the waist in an end-to-end configuration. With $N = 10$ particles, the total length of the particles is too long to form a single continuous deformation, as with $N = 4$. Instead, the particles assemble in a manner that favors end-to-end connections with the vesicle having multiple outward-facing lobes. Because the particles are concave and the shape of the vesicle accommodates their shape, the stiffness of the particle does not play as large of a role for the concave particles as it did for the convex particles.

We further characterize the effect of the number of particles on the deformations of the hinges in terms of the probability density of the hinge angle (Fig. 10). For convex particles, the hinge configurations are significantly affected by the number of particles. For $x = 0.146$, increasing the particle number induces a shift of the peak toward lower values. This is a consequence of the hinges causing a large deformation of the vesicle, which better accommodates the natural shape of the hinge, as shown in Fig. 9(a). For $x = 0.5$, increasing the particle number results in the emergence of multiple peaks. For concave particles, the number adsorbed has no appreciable effect on the hinge configuration at $x = 0.146$. For $x = 0.5$, increasing the particle number results in a modest shift of the peak toward the lower values.

IV. CONCLUSIONS

DNA origami nanoparticles, functionalized with lipid anchors, have the ability to interact with lipid membranes and induce curvature. The membranes can, in turn, promote the self-assembly of the nanoparticles due to effective interactions mediated by membrane bending.[21,22] Recent developments have opened the door to deformable DNA origami nanoparticles with controllable mechanical properties.[44] Such particles offer exciting opportunities because they provide new design parameters that can affect both the individual and collective behavior of membrane-anchored particles. In this work, we investigated the equilibrium properties of hinge-like particles adsorbed on membrane vesicles. We studied the effects of hinge stiffness, adhesive area fraction, patterning of the adhesive regions, and the number of particles.

For isolated particles, the effect of hinge stiffness is more pronounced for convex particles than for concave particles. This is a consequence of concave particles more easily conforming to the shape of the vesicle than convex particles. As the adhesive area fraction increases for both weak and strong concave particles, the particle induces a broad furrow that gives rise to a cashew-like vesicle shape. The convex particles generate larger membrane deformations, including inward membrane invaginations. Interestingly, the weak hinge with a large adhesive area fraction exhibits a bimodal distribution of the hinge angle, indicating that there are two prominent equilibrium configurations. These are associated with the particle being either straightened or bent. Straightening the particle is energetically unfavorable from the perspective of the particle, but it leads to a less pronounced membrane deformation. This behavior is not possible with rigid particles and demonstrates the nontrivial interplay between the mechanical properties of the particle and membrane.

For two hinge particles adsorbed on a vesicle, we again observed the possibility of multistable behavior. For convex particles with a small adhesive area fraction, the particles adopt either a side-by-side configuration or one in which they occupy opposite sides of the vesicle. Increasing the hinge stiffness promotes the side-by-side configuration, demonstrating that the mechanical properties of the particles can tune the resulting configurations. For the larger adhesive area fraction, the convex hinges form inward deformations and tend to be located on opposite sides of the vesicle. The more flexible hinges generate dumbbell-like vesicle shapes, while the stiffer hinges generate discocyte-like vesicle shapes. For concave particles, hinges with a small adhesive area fraction tend to broadly sample the surface with a preference to localize on opposite sides of the vesicle. Increasing the adhesive area fraction generates a bimodal distribution in which the particles align along a furrow circling the waist of cashew- or dumbbell-like vesicles, with the most likely configuration being an end-to-end aggregate. A comparison of the total energy and the PMF revealed the importance of entropic contributions to stable configurations associated with the particles residing far apart on the surface.

When multiple particles are adsorbed on a vesicle, the number and type of particles control the organization of particles and their collective impact on vesicle shape. The most pronounced and regular patterning of particles is observed for convex particles with a small adhesive area and concave particles with a large adhesive area. For large numbers of weak, convex particles with a small adhesive area, the particles assemble side-by-side into stable configurations that give rise to vesicles shaped either like a dumbbell or a three-way junction. Increasing the hinge stiffness promotes the dumbbell-like shape. Convex particles with a large adhesive area form prominent invaginations that tend to coalesce. For concave particles, the hinges with a large adhesive area induce dumbbell-like structures when a small number of particles circle the vesicle in an end-to-end configuration. When larger numbers of particles are adsorbed, the vesicles form multi-lobed shapes. Similar multi-lobed behavior has been observed in previous simulation studies of membranes with rigid BAR-family proteins. Noguchi observed that crescent rods generate a saddle shape, with outward buds stabilized by the side-by-side aggregation of rods with negative curvature.[65] Olinger *et al.* studied elongated curved nanoparticles adsorbed on vesicles and found that at weak adsorption strength, particles prefer side-by-side aggregation, while at strong adsorption strength, they self-assemble into asters to form a network spanning the vesicle.[42] A differentiating feature of our work is that the hinges can change their shape as they self-assemble, as characterized in Fig. 10.

Note that we consider vesicles of fixed size in this work. Both the vesicle size and the preferred angle of the hinge-like particles are expected to impact the membrane morphology, particle configurations, and self-assembly. By changing the vesicle size or preferred hinge angle, the mismatch between the curvature of the vesicle and the shape of the hinges can be tuned, which can lead to more or less pronounced deformations of the vesicle. The effect of vesicle size and the preferred shape of the hinge-like particle is an interesting topic for further exploration.

Our work here demonstrates that varying the mechanical properties and adhesive patterning of deformable particles can control

15 May 2024 15:20:43

Published under an exclusive license by AIP Publishing

membrane-mediated interactions between particles, their organization on the membrane, and the resulting membrane shapes. In contrast with particles of fixed shape, deformable particles offer new mechanical design properties that can be used to control their self-assembly. Such control may be useful for the self-assembly of DNA origami nanoparticles on membranes.

SUPPLEMENTARY MATERIAL

The supplementary material includes Fig. S1: Probability density of the hinge angle for a single convex particle adsorbed on a vesicle with $k_\theta = 5k_BT$.

ACKNOWLEDGMENTS

B.L. thanks the support of the National Natural Science Foundation of China (Grant No. 22303101). S.M.A. was supported by the National Science Foundation (Grant No. CBET-2217777).

AUTHOR DECLARATIONS

Conflict of Interest

The authors have no conflicts to disclose.

Author Contributions

Bing Li: Conceptualization (equal); Formal analysis (equal); Investigation (equal); Writing – original draft (lead); Writing – review & editing (equal). **Steven M. Abel**: Conceptualization (equal); Formal analysis (equal); Writing – original draft (supporting); Writing – review & editing (equal).

DATA AVAILABILITY

The data that support the findings of this study are available from the corresponding author upon reasonable request.

REFERENCES

[1]H. T. McMahon and J. L. Gallop, "Membrane curvature and mechanisms of dynamic cell membrane remodelling," Nature **438**, 590–596 (2005).
[2]J. Zimmerberg and M. M. Kozlov, "How proteins produce cellular membrane curvature," Nat. Rev. Mol. Cell Biol. **7**, 9–19 (2006).
[3]T. Baumgart, B. R. Capraro, C. Zhu, and S. L. Das, "Thermodynamics and mechanics of membrane curvature generation and sensing by proteins and lipids," Annu. Rev. Phys. Chem. **62**, 483–506 (2011).
[4]A. Frost, V. M. Unger, and P. De Camilli, "The BAR domain superfamily: Membrane-molding macromolecules," Cell **137**, 191–196 (2009).
[5]M. I. Mahmood, H. Noguchi, and K.-i. Okazaki, "Curvature induction and sensing of the F-BAR protein Pacsin1 on lipid membranes via molecular dynamics simulations," Sci. Rep. **9**, 14557 (2019).
[6]K. Takemura, K. Hanawa-Suetsugu, S. Suetsugu, and A. Kitao, "Salt bridge formation between the I-BAR domain and lipids increases lipid density and membrane curvature," Sci. Rep. **7**, 6808 (2017).
[7]A. Arkhipov, Y. Yin, and K. Schulten, "Membrane-bending mechanism of amphiphysin N-BAR domains," Biophys. J. **97**, 2727–2735 (2009).
[8]H. Yu and K. Schulten, "Membrane sculpting by F-BAR domains studied by molecular dynamics simulations," PLoS Comput. Biol. **9**, e1002892 (2013).
[9]M. Simunovic, A. Srivastava, and G. A. Voth, "Linear aggregation of proteins on the membrane as a prelude to membrane remodeling," Proc. Natl. Acad. Sci. U. S. A. **110**, 20396–20401 (2013).
[10]T. V. Sachin Krishnan, S. L. Das, and P. B. S. Kumar, "Transition from curvature sensing to generation in a vesicle driven by protein binding strength and membrane tension," Soft Matter **15**, 2071–2080 (2019).
[11]N. Ramakrishnan, J. H. Ipsen, M. Rao, and P. B. S. Kumar, "Organelle morphogenesis by active membrane remodeling," Soft Matter **11**, 2387–2393 (2015).
[12]P. W. K. Rothemund, "Folding DNA to create nanoscale shapes and patterns," Nature **440**, 297–302 (2006).
[13]S. M. Douglas, H. Dietz, T. Liedl, B. Högberg, F. Graf, and W. M. Shih, "Self-assembly of DNA into nanoscale three-dimensional shapes," Nature **459**, 414–418 (2009).
[14]D.-N. Kim, F. Kilchherr, H. Dietz, and M. Bathe, "Quantitative prediction of 3D solution shape and flexibility of nucleic acid nanostructures," Nucleic Acids Res. **40**, 2862–2868 (2011).
[15]M. Langecker, V. Arnaut, T. G. Martin, J. List, S. Renner, M. Mayer, H. Dietz, and F. C. Simmel, "Synthetic lipid membrane channels formed by designed DNA nanostructures," Science **338**, 932–936 (2012).
[16]A. J. Sodt and R. W. Pastor, "Molecular modeling of lipid membrane curvature induction by a peptide: More than simply shape," Biophys. J. **106**, 1958–1969 (2014).
[17]W. Wang, D. S. Arias, M. Deserno, X. Ren, and R. E. Taylor, "Emerging applications at the interface of DNA nanotechnology and cellular membranes: Perspectives from biology, engineering, and physics," APL Bioeng. **4**, 041507 (2020).
[18]S. Kocabey, S. Kempter, J. List, Y. Xing, W. Bae, D. Schiffels, W. M. Shih, F. C. Simmel, and T. Liedl, "Membrane-assisted growth of DNA origami nanostructure arrays," ACS Nano **9**, 3530–3539 (2015).
[19]A. Czogalla, D. J. Kauert, H. G. Franquelim, V. Uzunova, Y. Zhang, R. Seidel, and P. Schwille, "Amphipathic DNA origami nanoparticles to scaffold and deform lipid membrane vesicles," Angew. Chem., Int. Ed. **54**, 6501–6505 (2015).
[20]M. W. Grome, Z. Zhang, F. Pincet, and C. Lin, "Vesicle tubulation with self-assembling DNA nanosprings," Angew. Chem., Int. Ed. **57**, 5330–5334 (2018).
[21]H. G. Franquelim, A. Khmelinskaia, J. P. Sobczak, H. Dietz, and P. Schwille, "Membrane sculpting by curved DNA origami scaffolds," Nat. Commun. **9**, 811 (2018).
[22]A. Khmelinskaia, H. G. Franquelim, R. Yaadav, E. P. Petrov, and P. Schwille, "Membrane-mediated self-organization of rod-like DNA origami on supported lipid bilayers," Adv. Mater. Interfaces **8**, 2101094 (2021).
[23]B. J. Reynwar, G. Illya, V. A. Harmandaris, M. M. Müller, K. Kremer, and M. Deserno, "Aggregation and vesiculation of membrane proteins by curvature-mediated interactions," Nature **447**, 461–464 (2007).
[24]A. Saric and A. Cacciuto, "Fluid membranes can drive linear aggregation of adsorbed spherical nanoparticles," Phys. Rev. Lett. **108**, 118101 (2012).
[25]A. Saric and A. Cacciuto, "Mechanism of membrane tube formation induced by adhesive nanocomponents," Phys. Rev. Lett. **109**, 188101 (2012).
[26]A. H. Bahrami, R. Lipowsky, and T. R. Weikl, "Tubulation and aggregation of spherical nanoparticles adsorbed on vesicles," Phys. Rev. Lett. **109**, 188102 (2012).
[27]A. H. Bahrami, M. Raatz, J. Agudo-Canalejo, R. Michel, E. M. Curtis, C. K. Hall, M. Gradzielski, R. Lipowsky, and T. R. Weikl, "Wrapping of nanoparticles by membranes," Adv. Colloid Interface Sci. **208**, 214–224 (2014).
[28]A. H. Bahrami and T. R. Weikl, "Curvature-mediated assembly of Janus nanoparticles on membrane vesicles," Nano Lett. **18**, 1259–1263 (2018).
[29]B. J. Reynwar and M. Deserno, "Membrane-mediated interactions between circular particles in the strongly curved regime," Soft Matter **7**, 8567–8575 (2011).
[30]Y. Zhu, A. Sharma, E. J. Spangler, and M. Laradji, "Modes of adhesion of two Janus nanoparticles on the outer or inner side of lipid vesicles," Soft Matter **18**, 4689–4698 (2022).
[31]Y. Zhu, A. Sharma, E. J. Spangler, and M. Laradji, "Non-close-packed hexagonal self-assembly of Janus nanoparticles on planar membranes," Soft Matter **19**, 7591–7601 (2023).
[32]Y. Zhu, A. Sharma, E. J. Spangler, J.-M. Y. Carrillo, P. B. S. Kumar, and M. Laradji, "Lipid vesicles induced ordered nanoassemblies of Janus nanoparticles," Soft Matter **19**, 2204–2213 (2023).

15 May 2024 15:20:43

Published under an exclusive license by AIP Publishing

[33]T. R. Weikl, M. M. Kozlov, and W. Helfrich, "Interaction of conical membrane inclusions: Effect of lateral tension," Phys. Rev. E **57**, 6988–6995 (1998).
[34]A. B. Petrova, C. Herold, and E. P. Petrov, "Conformations and membrane-driven self-organization of rodlike fd virus particles on freestanding lipid membranes," Soft Matter **13**, 7172–7187 (2017).
[35]M. Simunovic and G. A. Voth, "Membrane tension controls the assembly of curvature-generating proteins," Nat. Commun. **6**, 7219 (2015).
[36]M. Simunovic, E. Evergren, I. Golushko, C. Prévost, H. F. Renard, L. Johannes, H. T. McMahon, V. Lorman, G. A. Voth, and P. Bassereau, "How curvature-generating proteins build scaffolds on membrane nanotubes," Proc. Natl. Acad. Sci. U. S. A. **113**, 11226–11231 (2016).
[37]M. Simunovic, A. Saric, J. M. Henderson, K. Y. C. Lee, and G. A. Voth, "Long-range organization of membrane-curving proteins," ACS Cent. Sci. **3**, 1246–1253 (2017).
[38]S. K. Ghosh, A. G. Cherstvy, E. P. Petrov, and R. Metzler, "Interactions of rod-like particles on responsive elastic sheets," Soft Matter **12**, 7908–7919 (2016).
[39]F. Bonazzi and T. R. Weikl, "Membrane morphologies induced by arc-shaped scaffolds are determined by arc angle and coverage," Biophys. J. **116**, 1239–1247 (2019).
[40]H. Noguchi, "Membrane shape deformation induced by curvature-inducing proteins consisting of chiral crescent binding and intrinsically disordered domains," J. Chem. Phys. **157**, 034901 (2022).
[41]E. J. Spangler, A. D. Olinger, P. B. S. Kumar, and M. Laradji, "Binding, unbinding and aggregation of crescent-shaped nanoparticles on nanoscale tubular membranes," Soft Matter **17**, 1016–1027 (2021).
[42]A. D. Olinger, E. J. Spangler, P. B. S. Kumar, and M. Laradji, "Membrane-mediated aggregation of anisotropically curved nanoparticles," Faraday Discuss. **186**, 265–275 (2016).
[43]F. Bonazzi, C. K. Hall, and T. R. Weikl, "Membrane morphologies induced by mixtures of arc-shaped particles with opposite curvature," Soft Matter **17**, 268–275 (2021).
[44]L. F. Zhou, A. E. Marras, H. J. Su, and C. E. Castro, "DNA origami compliant nanostructures with tunable mechanical properties," ACS Nano **8**, 27–34 (2014).
[45]A. E. Marras, L. Zhou, H. J. Su, and C. E. Castro, "Programmable motion of DNA origami mechanisms," Proc. Natl. Acad. Sci. U. S. A. **112**, 713–718 (2015).
[46]E. Büber, T. Schröder, M. Scheckenbach, M. Dass, H. G. Franquelim, and P. Tinnefeld, "DNA origami curvature sensors for nanoparticle and vesicle size determination with single-molecule FRET readout," ACS Nano **17**, 3088–3097 (2023).
[47]J. Gomez-Llobregat, F. Elias-Wolff, and M. Linden, "Anisotropic membrane curvature sensing by amphipathic peptides," Biophys. J. **110**, 197–204 (2016).
[48]H. Noguchi, "Curvature sensing of curvature-inducing proteins with internal structure," Phys. Rev. E **109**, 024403 (2024).
[49]N. Nambiar, Z. A. Loyd, and S. M. Abel, "Particle deformability enables control of interactions between membrane-anchored nanoparticles," J. Chem. Theory Comput. **20**, 1732–1739 (2024).
[50]B. Li and S. M. Abel, "Membrane-mediated interactions between hinge-like particles," Soft Matter **18**, 2742–2749 (2022).
[51]Y. Gao and Y. Yu, "How half-coated Janus particles enter cells," J. Am. Chem. Soc. **135**, 19091–19094 (2013).
[52]Y. Kantor and D. R. Nelson, "Crumpling transition in polymerized membranes," Phys. Rev. Lett. **58**, 2774–2777 (1987).
[53]G. Gompper and D. M. Kroll, "Random surface discretizations and the renormalization of the bending rigidity," J. Phys. I **6**, 1305–1320 (1996).
[54]D. R. Nelson, T. Piran, and S. Weinberg, *Statistical Mechanics of Membranes and Surfaces*, 2nd ed. (World Scientific, Singapore, 2004).
[55]D. M. Kroll and G. Gompper, "The conformation of fluid membranes: Monte Carlo simulations," Science **255**, 968–971 (1992).
[56]B. Li and S. M. Abel, "Shaping membrane vesicles by adsorption of a semiflexible polymer," Soft Matter **14**, 185–193 (2018).
[57]A. Saric and A. Cacciuto, "Self-assembly of nanoparticles adsorbed on fluid and elastic membranes," Soft Matter **9**, 6677–6695 (2013).
[58]S. Mirzaeifard and S. M. Abel, "Confined semiflexible polymers suppress fluctuations of soft membrane tubes," Soft Matter **12**, 1783–1790 (2016).
[59]C. Micheletti, D. Marenduzzo, and E. Orlandini, "Polymers with spatial or topological constraints: Theoretical and computational results," Phys. Rep. **504**, 1–73 (2011).
[60]B. Li, Z. Y. Sun, L. J. An, and Z. G. Wang, "Influence of topology on the free energy and metric properties of an ideal ring polymer confined in a slit," Macromolecules **48**, 8675–8680 (2015).
[61]J. Kästner, "Umbrella sampling," Wiley Interdiscip. Rev.: Comput. Mol. Sci. **1**, 932–942 (2011).
[62]B. Li, Z. Sun, L. An, and Z. G. Wang, "The scaling behavior of the second virial coefficient of linear and ring polymer," Sci. China Chem. **59**, 619–623 (2016).
[63]A. Vahid, A. Šarić, and T. Idema, "Curvature variation controls particle aggregation on fluid vesicles," Soft Matter **13**, 4924–4930 (2017).
[64]G. Chauhan, M. L. Simpson, and S. M. Abel, "Crowding-induced interactions of ring polymers," Soft Matter **17**, 16–23 (2021).
[65]H. Noguchi, "Membrane tubule formation by banana-shaped proteins with or without transient network structure," Sci. Rep. **6**, 20935 (2016).

15 May 2024 15:20:43

Published under an exclusive license by AIP Publishing